



Published in final edited form as:

Nature. 2017 August 17; 548(7667): 338–342. doi:10.1038/nature23450.

m⁶A mRNA methylation controls T cell homeostasis by targeting IL-7/STAT5/SOCS pathway

Hua-Bing Li^{1,*.§}, Jiyu Tong^{1,2,*}, Shu Zhu^{1,*}, Pedro J. Batista³, Erin E. Duffy^{4,5}, Jun Zhao^{1,6}, Will Bailis¹, Guangchao Cao^{1,2}, Lina Kroehling¹, Yuanyuan Chen^{1,7}, Geng Wang¹, James P. Broughton³, Y. Grace Chen³, Yuval Kluger⁶, Matthew D. Simon^{4,5}, Howard Y. Chang³, Zhinan Yin^{2,§}, and Richard A. Flavell^{1,8,§}

¹Department of Immunobiology, Yale University School of Medicine, New Haven, CT 06520

²The First Affiliated Hospital, Biomedical Translational Research Institute and Guangdong Province Key Laboratory of Molecular Immunology and Antibody Engineering, Jinan University, Guangzhou 510632, P. R. China

³Dynamic Regulomes, Stanford University, Stanford, CA 94305, USA

⁴Department of Molecular Biophysics & Biochemistry, Yale University, New Haven, CT 06511, USA

⁵Chemical Biology Institute, Yale University, West Haven, CT 06516, USA

⁶Department of Pathology, Yale University School of Medicine, New Haven, CT 06520

⁷Institute of Surgical Research, Daping Hospital, the Third Military Medical University, Chongqing, China 400038

⁸Howard Hughes Medical Institute, Chevy Chase, MD 20815-6789, USA

Abstract

*N*⁶-methyladenosine (m⁶A) is the most common and abundant messenger RNA modification, modulated by ‘writers’, ‘erasers’ and ‘readers’ of this mark^{1,2}. *In vitro* data have shown that m⁶A

Users may view, print, copy, and download text and data-mine the content in such documents, for the purposes of academic research, subject always to the full Conditions of use: http://www.nature.com/authors/editorial_policies/license.html#terms Reprints and permissions information is available at www.nature.com/reprints

[§]Corresponding Authors: Richard A. Flavell, Ph.D., FRS, Department of Immunobiology, Yale University School of Medicine, 300 Cedar Street, TAC S-569, New Haven, CT 06520, (203) 737-2216 (phone), (203) 737-2958 (FAX), richard.flavell@yale.edu. Hua-Bing Li, Ph.D., Department of Immunobiology, Yale University School of Medicine, 300 Cedar Street, TAC S-569, New Haven, CT 06520, huabing.li@yale.edu. Zhinan Yin, Ph.D., The First Affiliated Hospital, Biomedical Translational Research Institute and Guangdong Province Key Laboratory of Molecular Immunology and Antibody Engineering, Jinan University, Guangzhou 510632, P. R. China., zhinan.yin@yale.edu.

*These authors contributed equally to this work.

§These authors jointly supervised this work.

Correspondence and requests for materials should be addressed to R.A.F. (richard.flavell@yale.edu), H.-B.L. (huabing.li@yale.edu) or Z.Y. (zhinan.yin@yale.edu).

Supplementary Information is available in the online version of the paper.

Author Contributions H.-B. L. conceived the project. H.-B. L., J. T., S. Z., P.B., E.E.D., W.B., G.C., Y. C., G.W., J.P.B. and Y.G.C. performed the experimental work. J.Z., L.K., M.D.S. and P.B. analyzed the RNA-Seq, Ribo-Profiling, s4U-Seq, m⁶A-Seq data and performed the statistical analysis. H.Y.C., M.D.S., Y.K., and Z.Y. provided key suggestions. H.-B. L. and R.A.F. designed the study, analyzed the data and wrote the manuscript. R.A.F supervised the study.

The authors declare no competing financial interests.

influences all fundamental aspects of mRNA metabolism, mainly mRNA stability, to determine stem cell fates^{3,4}. However, its *in vivo* physiological function in mammals and adult mammalian cells is still unknown. Here we show that deletion of m⁶A ‘writer’ protein METTL3 in mouse T cells disrupts T cell homeostasis and differentiation. In a lymphopenic mouse adoptive transfer model, naïve *Mettl3* deficient T cells failed to undergo homeostatic expansion and remarkably remained in the naïve state up through 12 weeks, thereby preventing colitis. Consistent with these observations, the mRNAs of SOCS family genes encoding STAT- signaling inhibitory proteins, *Socs1*, *Socs3* and *Cish*, were marked by m⁶A, exhibited slower mRNA decay and increased mRNAs and protein expression levels in *Mettl3* deficient naïve T cells. This increased SOCS family activity consequently inhibited IL-7 mediated STAT5 activation and T cell homeostatic proliferation and differentiation. We also found that m⁶A plays important roles for inducible degradation of *Socs* mRNAs in response to IL-7 signaling in order to reprogram Naïve T cells for proliferation and differentiation. Our study elucidates for the first time the *in vivo* biological role of m⁶A modification in T cell mediated pathogenesis and reveals a novel mechanism of T cell homeostasis and signal-dependent induction of mRNA degradation.

T cell differentiation and proliferation represent an exceptionally simple and tractable model system to understand the general principles of cellular specification and gene regulation. Alpha beta naïve T cells can differentiate and proliferate into distinct functional T helper effector subset cells in response to defined cytokines *in vitro* and different micro-environmental signals *in vivo*^{5,6}. As m⁶A plays an essential role during the cell fate patterning of embryonic stem cells *in vitro*, we hypothesized m⁶A might be an important regulator of T helper (Th) differentiation. To study the *in vivo* functions of m⁶A, we generated conditional knockout mice for the m⁶A writer protein, METTL3 (Extended Data Fig. 1a), as *Mettl3* knockout (KO) mice are embryonic lethal³. CD4+ T cells from CD4-CRE conditional *Mettl3*^{lox/Lox} mice displayed absence of both METTL3 and its associated METTL14 proteins (Extended Data Fig. 1b). Concomitantly, the overall RNA m⁶A methylation levels in KO cells were decreased to roughly 28% of that in wild type (WT) cells (Extended Data Fig. 1c). Characterization of murine immune cell populations in the steady state revealed that T cell homeostasis was abnormal in spleen and lymph nodes, but not thymus, exhibited by the fact that naïve T cell numbers from lymph nodes were increased (Extended Data Fig. 1d–g).

To characterize the possible defects of the *Mettl3* KO naïve T cells, we utilized the defined *in vitro* TCR-dependent T cell differentiation system and found that *Mettl3* deficient naïve T cells exhibited reduction of Th1 and Th17 cells, an increase in Th2 cells, and no changes in Treg cells relative to WT naïve T cells (Extended Data Fig. 2a, b). We also saw no significant differences in proliferation and apoptosis between the WT and KO naïve T cells in these cultures (Extended Data Fig. 2c, d). Together, these findings suggest that m⁶A modification plays an important role during CD4+ T cell differentiation, but not on T cell apoptosis and TCR-mediated proliferation.

Upon adoptive transfer into lymphopenic mice, naïve T cells normally undergo homeostatic expansion in response to the elevated IL-7 levels in such mice and differentiate into effector T cells, causing colitis⁷. To study how *Mettl3* regulates naïve T cell homeostasis *in vivo*, we

adoptively transferred CD4⁺CD25⁻CD45RB^{hi} naïve T cells into *Rag2*^{-/-} mice, and found that mice receiving KO naïve T cells (*Mettl3*^{-/-} recipients) showed no signs of disease up to 12 weeks after transfer. *Mettl3*^{-/-} recipients continued to gain weight throughout the experiment, while control mice that received WT naïve T cells (*Mettl3*^{+/+} recipient) began losing weight at the 5th week after transfer (Fig. 1a). *Mettl3*^{-/-} recipients exhibited no colitis upon endoscopy, displayed normal colon length, and were found to have reduced spleen and lymph node sizes compared to WT control mice at the 8th week after transfer (Fig. 1b, Extended Data 3a, b). When analyzed by FACS, *Mettl3*^{-/-} CD45.2 CD4⁺ donor T cells were nearly undetectable in recipient colons (Fig. 1d), as well as in the spleen, but instead remained in peripheral and mesenteric lymph nodes, while WT donor T cells were found in large numbers in all lymphoid organs of the recipients (Extended Data Fig. 3c, d). Haematoxylin and Eosin (H&E) staining and analysis of colons also confirmed that the *Mettl3* KO T cells caused no T cell infiltration and inflammation, while WT T cells caused severe colonic inflammation and disrupted colon structure (Fig. 1c). Remarkably, FACS analysis further revealed that the vast majority of transferred *Mettl3*^{-/-} T cells recovered from the peripheral lymph nodes still displayed their original naïve T cell marker CD45RB⁺ as long as 12 weeks after transfer into *Rag2*^{-/-} mice, while the transferred WT cells differentiated into the effector/memory T cells (CD45RB^{low}) which mediated the pathology in this model (Fig. 2a).

We next sought to investigate whether *Mettl3*^{-/-} naïve T cells were capable of proliferation and could demonstrate normal survival after transfer into *Rag2*^{-/-} mice⁸. Using CellTrace labeling of the transferred naïve T cells, proliferation of WT cells was observable beginning week 2, whereas *Mettl3* KO T cells retained a naïve phenotype and proliferated slowly. Four weeks after transfer, over 90% of WT cells had differentiated into effector/memory cells, while most of the *Mettl3* KO T cells remained naïve and failed to display increased proliferation (Fig. 2b, c). Despite starting with a similar number of cells, WT cells proliferated over 50 times more than *Mettl3* KO cells by the second week, and over 400 times more by week four (Fig. 2d). No differences in apoptosis were observed between *Mettl3* KO and WT T cells (Extended Data Fig. 3e), suggesting the differences in cell number were not due to defects in cell viability.

To establish that m⁶A directly controls T cell homeostatic expansion, we re-introduced WT *Mettl3* gene or m⁶A catalytic dead *Mettl3* gene back into *Mettl3* KO naïve T cells, and showed that the WT *Mettl3* gene, but not m⁶A catalytic dead *Mettl3*, could largely rescue the differentiation defects of *Mettl3* KO naïve T cells *in vivo* (Extended Data Fig. 3f, g). Furthermore, we also generated an additional CD4-CRE conditional mouse line for *Mettl14*, an essential m⁶A catalytic partner for *Mettl3* in the same m⁶A ‘writer’ complex. *Mettl14* KO mice showed an identical phenotype to *Mettl3* KO mice. Specifically, 4 weeks after transfer into *Rag2*^{-/-} mice *Mettl14* KO naïve T cells remained in the naïve state (Fig. 2e), the mice displayed smaller lymphoid organs, and expanded less than transferred WT naïve T cells (Extended Data Fig. 4a–d). Taken together, our data suggest that m⁶A RNA modification is required not only for Th cell differentiation and proliferation *in vivo*, but also for T cells to properly exit the naïve “progenitor” state.

Peripheral T cell pools are maintained by complex mechanisms, and naïve T cell homeostasis and survival is mainly sustained by the IL-7/STAT5 and self-peptide-MHC/TCR signaling axes⁹. It is well established that the elevated levels of IL-7 in lymphopenic mice induce extensive homeostatic proliferation and differentiation of naïve T cells after adoptive transfer¹⁰. We hypothesized that the IL-7 receptor and its downstream molecular pathway were compromised in *Mettl3* KO cells. Consistently, we observed dramatically decreased JAK1 and STAT5 phosphorylation levels in KO naïve T cells upon IL-7 stimulation (Fig. 3a). Moreover, basal ERK and AKT, but not NFκB, phosphorylation was found to be elevated in KO naïve T cells, with TCR stimulation only minimally enhancing ERK and AKT signaling. These findings are consistent with the observation that *Mettl3* KO naïve T cells proliferate normally *ex vivo* after TCR stimulation, indicating the limited proliferation found after adoptive transfer to lymphopenic mice was driven by defects in STAT5 phosphorylation, while their long term survival in these recipients was maintained by elevated basal ERK and AKT signaling. We conclude that m⁶A controls the balance of the two essential signaling pathways to control the T cell homeostasis, IL-7 mediated JAK-STAT signaling and TCR mediated ERK/AKT signaling, thus uncoupling T cell proliferation from cell survival.

To further explore the molecular mechanism underlying the IL-7 signaling pathway defects, we performed an RNA-Seq analysis on the naïve T cells isolated from *Mettl3* KO mice and littermate control WT mice. Consistent with our biochemical observations, the JAK-STAT and TCR signaling pathways were among the top up-regulated KEGG pathways (Extended Data Fig. 5a, b & Supplementary Information Table 3). Notably, three Suppressor of cytokine signaling (SOCS) family genes (*Socs1*, *Socs3* and *Cish*) were among the most significantly up-regulated genes. RNA-Seq results were validated by qPCR and western blot, confirming that *Socs1*, *Socs3* and *Cish* were over-expressed and SOCS1 in particular showed even higher relative expression in *Mettl3* KO naïve T cells (Fig. 3c, d), while other important genes in IL-7 signaling pathways did not change (Extended Data Fig. 5c). SOCS proteins are the key physiological inhibitors of JAK-STAT signaling pathways and play important roles in T cell proliferation and differentiation^{11,12}. In particular, SOCS1 is a well-known negative regulator of IL-7 signaling, and SOCS3 and CISH also inhibit STAT5 phosphorylation, and T cell proliferation, while promoting ERK activity by binding to RasGAP^{13,14,15,16,17}. Consistently, siRNA mediated *Socs1* knockdown partially rescued the *in vivo* differentiation defects of *Mettl3* KO Naïve T cells 4 weeks after adoptive transfer into *Rag2*^{-/-} mice (Fig. 3e, Extended Data Fig. 5d). Altogether, overexpression of SOCS1, SOCS3 and CISH in *Mettl3* KO cells likely synergistically suppresses IL-7/STAT5 signaling, while enhancing ERK and AKT signaling, to inhibit naïve T cell proliferation and differentiation but maintain its survival.

RNA m⁶A methylation is understood to affect RNA stability, with *Mettl3* deletion resulting in loss of the m⁶A marker and in turn a slower RNA decay of m⁶A targets^{2-4,18}. To assess whether loss of *Mettl3* resulted in decreased m⁶A methylation of SOCS family member mRNA, we performed genome-wide m⁶A methylation profiling using m⁶A-RIP-Seq with WT CD4⁺ T cells, and found that *Socs1* and *Socs3* mRNA 3' UTRs have highly enriched and specific m⁶A peaks (Fig. 3f), which is consistent with published mouse ESC and mouse dendritic cell m⁶A-Seq datasets^{4,19} (Extended Data Fig. 5e). We confirmed by m⁶A RNA-IP

qPCR that *Socs1*, *Socs3* and *Cish* mRNAs were bona fide m⁶A targets, and that m⁶A was lost in *Mettl3* KO naïve T cells (Fig. 3g). Next, we performed RNA decay assays and found that *Socs1*, *Socs3* and *Cish* mRNA levels were all increased in *Mettl3*^{-/-} cells in comparison to WT cells 2 hours after Actinomycin-D treatment (Fig. 3h). m⁶A was also reported to affect RNA splicing and translation^{2-4,18}. To address those possibilities, we first performed genome-wide Ribosome profiling, and found that ribosome occupancy and the calculated translation efficiency were not affected for all the related genes in *Mettl3* KO cells versus WT cells (See Methods and Extended Data Fig. 6a-d & Supplementary Information Table 4); Next, we analyzed our deep RNA-Seq data, and did not find any splicing differences between *Mettl3* KO and WT cells, suggesting that the Naïve T cell homeostasis defect is mainly due to m⁶A mediated degradation, rather than splicing or translation. Taken together, loss of m⁶A modification in *Mettl3* KO naïve T cells leads to increased *Socs1*, *Socs3* and *Cish* mRNA half-life and proteins levels, thus suppressing the IL-7/STAT5 signaling pathway.

mRNA levels are tightly regulated by both transcription and degradation²⁰. While the abundance of most of transcripts are mainly controlled by transcription rate, it has been shown that the mRNA levels of a minority of genes (~17%) are significantly regulated by mRNA degradation rates, notably immediate-early inducible genes^{21,22}. *Socs* genes are well-known immediate-early genes induced upon IL-7 stimulation^{11,12}, thus we hypothesized that m⁶A specifically targets “signal-dependent immediate-early genes” for degradation. Interestingly, we found that up-regulated genes (including *Socs1* and *Socs3*) in *Mettl3* KO Naïve T cells were significantly enriched in the degradation controlled group of genes from LPS stimulated dendritic cells (chi square test, p<0.0001, Extended Data fig. 7a)^{20,21}. In addition, using the RNA decay assay we found that mRNAs of all the three *Socs* genes were degraded faster upon IL-7 stimulation as early as 10min after IL-7 stimulation comparing to control treatment in WT cells, while the accelerated mRNA degradation upon IL-7 stimulation is abrogated in *Mettl3* KO naïve T cells (Extended Data Fig. 7b). To extend our observation genome-wide and estimate the rates of synthesis and degradation, we conducted a time course s⁴U-Seq with IL-7 induction and found a cluster of 34 transcripts including *Cish*, *Socs1* and *Socs3* are increased in *Mettl3* KO relative to WT cells and show similar kinetics of induction (Fig. 4a, b, See Methods and Extended Data Fig. 8a-c & Supplementary Information Table 5)²³. This analysis also confirmed that the estimated degradation rates were lower in *Mettl3* KO cells for *Socs* transcripts after IL-7 induction (Fig. 4c, d). We conclude that m⁶A targets a group of immediate-early inducible genes including *Socs1*, *Socs3* and *Cish* for rapid mRNA degradation upon IL-7 stimulation, allowing IL-7-JAKs signaling to activate the downstream target STAT5, to initiate the re-programming of the naïve T cells for differentiation and proliferation.

T cell homeostasis is essential to maintain the T cell pool size and forms the basis for adaptive immunity. Rather than the findings of m⁶A functions in ESCs, here we have revealed a different strategy, whereby m⁶A targets mRNAs encoding signaling proteins which control the “gatekeeper” IL-7 signal in naïve T cells, the progenitors of the adaptive immune system. Thus these targets expand the scope of m⁶A biology and enables RNA modification to impact critical dynamic signaling systems and response to external stimuli that maintain homeostasis. Specifically, using *Mettl3* and *Mettl14* conditional knockout

mice, our current study demonstrates a novel mechanism whereby m⁶A functions *in vivo* to control T cell homeostasis by inducible degradation of *Socs* gene family mRNA, and consequently relieving the block on IL-7 signaling and T cell proliferation (Extended Data Fig. 9). Our study implies that m⁶A represents an evolutionarily conserved mechanism to specifically control the degradation rates of a group of immediate-early response genes in response to various environmental stimuli. Our study illustrates how this important epitranscriptomic marker not only plays an essential role in development, but that m⁶A modifications act as a critical regulator of immune cell homeostasis and function, opening new avenues of investigation into the function of m⁶A in human health and disease. Since T cells regulate the entire adaptive immune response, this has broad implications. These findings further suggest that T cell specific delivery of m⁶A-modifying agents might be an effective therapeutics to alleviate various autoimmune diseases.

Methods

Mice

Mettl3 and *Mettl14* conditional knockout mice were both generated by inserting two lox sites into the first and the last introns using the CRISPR/cas9 based genome-editing system as previously described (Extended Data Fig. 1a)²⁴. The gRNA and donor oligos used for *Mettl3* left side lox were: *agtgcctgcatggaatgaa* agg, and *ag*t*a*ggtctctggaaaatccaggattatttggcaaaacagcaagtgctgcatggaatgaa* *ataacttcgtataatgatgctatacgaagttat* *aggatgatagagtaacgctggctcagagaccctgctgaagtgaagatgtgtgctagcg*a*t*g*; for *Mettl3* right side lox: *atacattctgtagtctaga* tgg, and *cc*c*c*caaaaaccctttatggacaaagacagatgtcactgagttgt* *atacattctgtagtctaga* *ataacttcgtataatgatgctatacgaagttat* *tggcttaagctttaccagaatctacaacattcattagaacccaaagggtgttcttaaagtc*t*a*a*. The gRNA and donor oligos used for *Mettl14* left side lox were: *cataaagtggttcacatgaa* ggg, and *aa*t*g*aagctgagtcacatctctgtgagagcaggagatacatgtagtacataaagtggttcacatgaa* *ataacttcgtataatgatgctatacgaagttat* *gggctttgcttctgtgttactgcttctgatccaactgtattcattaccattggcgaca*g*g*g*. for *Mettl14* right side lox were: *tacatagatgaggaacaata* agg, and *at*t*g*tgtattaaaatattcttcttaagtgtattcttaacaacacaatacatagatgaggaacaata* *ataacttcgtataatgatgctatacgaagttat* *aggatgatatgtaacaaaagctataatctagaacgagaacaaggtatgtgcatatggacctt*t*t*a*. The donor oligos were synthesized by IDT with 5' - and 3' -ends modified by Phosphorothioate bonds to increase the oligo stability after delivered into mouse embryos. The pups born were genotyped and the PCR products were sequenced to validate intact integration of the lox sequences into the right genome loci.

We crossed floxed *Mettl3* mice or *Mettl14* with CD4-CRE mice to obtain conditional knockout mice. The CD4-CRE mice has been purchased from the Jackson laboratory and been fully backcrossed to C57BL/6 mice from the Charles River laboratories (over more than 10 generations).

Mettl3-fl/fl without CD4-CRE, or only CD4-CRE mice had both been used as WT controls for *Mettl3*-fl/fl; CD4-CRE mice, and we found there were no signs of differences using

either one regarding our observed phenotypes. Thereafter, we only used *Mettl3*-fl/fl as WT controls for *Mettl3*-fl/fl; CD4-CRE KO mice for most of the experiments reported here. All the KO and WT mice were littermates and co-housed for any experiments described. All the mice were bred and maintained under specific pathogen-free conditions at the animal facility of Yale University School of Medicine. Animal procedures were approved by the Institutional Animal Care and Use Committee of Yale University. Both female and male mice were used in experiments. Wherever possible, preliminary experiments were performed to determine requirements for sample size, taking into account resources available and ethical, reductionist animal use. Exclusion criteria such as inadequate staining or low cell yield due to technical problems were pre-determined. Animals were assigned randomly to experimental groups. Each cage contained animals of all the different experimental groups.

Reagents and antibodies

The detailed information on all reagents and antibodies used in this study are listed in Supplementary Information table 1.

CD45RB^{hi} adoptive transfer colitis, endoscopic and histologic analysis

We performed the experiment as described ^{7,25}. Briefly, pure CD4+CD25⁻CD45RB^{hi} naïve T cells were sorted from WT and *Mettl3* or *Mettl14* KO mice by FACS, washed twice with PBS, counted, and intravenously injected 0.5 million cells into each *Rag2*^{-/-} recipient mice. The recipient mice were monitored and weighted each week.

At week 7, colon colitis was visualized using Coloview system (Karl Storz, Germany). Briefly, colitis score was evaluated considering the consistence of stools, granularity of the mucosal surface, translucency of the colon, fibrin deposit and vascularization of the mucosa (0–3 points for each parameter). Haematoxylin and eosin staining were performed on paraffin sections of colon previously fixed in Bouin's fixative solutions.

Cell Proliferation and apoptosis assay

To trace T cell homeostatic proliferation *in vivo*, we labeled the FACS purified CD4+CD25⁻CD45RB^{hi} naïve cells with CellTrace (ThermoFisher Scientific, C34557) before I.V. injections ⁸. We then intravenously injected 0.5 million cells into each *Rag2*^{-/-} recipient mice. We analyzed the mice at 1 week, 2 week, 4 week and 10 weeks respectively after injection by FACS using the naïve T cell marker CD45RB for differentiation, and CellTrace violet for proliferation.

For apoptosis assay, we stained the *in vitro* cultured cells or cells from mice with Annexin V and 7-AAD and analyzed by FACS, in which double negative cells are viable cells, while Annexin V⁺ or double positive cells are apoptotic cells.

T cell *ex vivo* differentiation

We FACS sorted CD4⁺ C62L+CD44^{low} cells with FACS Aria II Cell Sorter (BD Biosciences) and activated them with plate-bound monoclonal antibodies to CD3 (10 µg ml⁻¹, 145-2C11) and CD28 (1–2 µg ml⁻¹, PV-1) in the presence of mouse recombinant cytokines and blocking antibodies. Specifically, Th1 direction with IL-12 (10ng ml⁻¹) and

antibody to IL-4 (11B11, 10 $\mu\text{g ml}^{-1}$); Th2 direction with IL4 (10 ng ml⁻¹) and antibody to IFN- γ (XMG1.2, 10 $\mu\text{g ml}^{-1}$); Th17 with IL-6 (20 ng ml⁻¹), IL-23 (20 ng ml⁻¹), and antibodies to IFN- γ (XMG1.2, 10 $\mu\text{g ml}^{-1}$) and IL-4 (11B11, 10 $\mu\text{g ml}^{-1}$); iTreg with TGF- β (2 ng ml⁻¹), IL-2 (50 U ml⁻¹), IL-23 (20 ng ml⁻¹), and antibodies to IFN- γ (XMG1.2, 10 $\mu\text{g ml}^{-1}$) and IL-4 (11B11, 10 $\mu\text{g ml}^{-1}$). All cytokines were purchased from R&D. Click's (Irvine Scientific) or RPMI (SIGMA-ALDRICH) (when indicated) media were supplemented with 10% FBS, L-glutamine (2 mM), penicillin (100 U ml⁻¹) and β -mercaptoethanol (40 nM). After 4 days of culture, the cells were analyzed by FACS.

Signaling Assay

Naïve T cells were isolated by FACS, counted, and 1 million cells in cell culture media were plated on each well of 48 well plate. 10 μg of IL-7, or IL-2, or 0.2 μl of CD3/CD28 beads (ThermoFisher Scientific, 11452D) were added into the media, mixed and incubated in 37 °C incubator. Cells were harvested before adding cytokines or antibody beads (t=0), or 30 min (t=30), or 60 min (t=60) after adding the cytokines or antibody beads. The cells were lysed on ice for 30 min in RIPA buffer (ThermoFisher Scientific, 89901) with protease inhibitor cocktails (ThermoFisher Scientific, 78437) and phosphatase inhibitor cocktails (ThermoFisher Scientific, 78428). The supernatant were subjected western blot.

RNA-Seq

We isolated CD4⁺ cells using StemCell mouse CD4⁺ Kit (StemCell Technologies, Catalog # 19852) from spleen and lymph nodes. Then pure CD4⁺CD25⁻CD45RBhi naïve T cells were isolated by FACS sorting. We used two pairs of WT and KO mice for the experiment. Total RNAs were isolated with Direct-zol RNA MicroPrep kits (Zymo Research, R2062). Yale Center for Genome Analysis (YCGA) processed the total RNA by Ribo-Zero rRNA removal kit, constructed the libraries, and subject them to standard illumine HiSeq2000 sequencing, and obtained >40 million reads for each samples.

Raw RNA sequencing reads were aligned to the mouse genome (mm10, GRCm38) with Tophat²⁶. Gene expression levels were measured by Cufflinks and differential analysis was performed with Cuffdiff²⁷. Genes were considered significantly differentially expressed if showing 1.5 fold change and <0.01 p-value. Gene set analysis was performed and enriched KEGG pathways were obtained through online bioinformatics tools²⁸. Volcano plot and pathway plot were generated with R package “ggplot2”²⁹. We used CuffDiff and rMATS to analyze the possible splicing difference events, and did not find any significant difference between *Mettl3* KO and WT samples³⁰.

RT-qPCR

Total RNA was isolated from Naïve T cells as described in ‘RNA-Seq’ section, then reverse transcribed using High-Capacity cDNA Reverse Transcription Kit (ThermoFisher Scientific, 4368814). Primers used for qPCR are included in Supplementary Information table 2. All qPCRs were run on Bio-Rad CFX96 real-time system using iTaq Universal SYBR Green Supermix (Bio-Rad, #1725124). Actin-b was used as internal control to normalize the data across different samples.

RNA degradation assay

Purified Naïve T cells by FACS sorting were plated on 96-well plate with 0.5 million cells per well. Actinomycin-D (Sigma-Aldrich, A1410) was added to a final concentration of 5 μ M, and cells were harvested before, or 2hrs after adding actinomycin-D. Then the cells were processed as described in 'RT-qPCR' section, except that the data were normalized to the t=0 time point.

For signaling dependent degradation assay, we first treat the naïve T cells with actinomycin-D for 1hr to fully inhibit transcription, then add IL-7 (10 μ g/mL) or PBS as control into each well of the cells. Cells were lysed with Trizol LS at 0, 10min, 20min, 30min, Or 45min after IL-7 addition.

HPLC quantification of m⁶A levels

RNA was collected with RLT buffer (Qiagen) according to manufactures instruction. Two rounds of poly(A) selection were performed using PolyA purist Mag kit (Ambion). 200 ng of Poly(A)-selected RNA was digested with 1 unit of Nuclease P1 in 50 mM NH₄OAc at 37°C for 1 hour, and sample was cleared on a 0.22 μ m filter. HPLC was performed on an Agilent 1290 Infinity UPLC system coupled to the Agilent 6490 Triple Quad mass spectrometer with the iFunnel. For the LC, the A solvent is water with 0.1% formic acid and B solvent is acetonitrile with 0.1% formic acid. The MS is in positive mode, scanning for the AMP and m⁶A product ion of 136 and 150.1, respectively. Samples were run in duplicate, and m⁶A/A ratios calculated.

m⁶A RNA-IP-qPCR & m⁶A RNA-IP-Seq

Total RNA was isolated with TRIZOL, according to manufactures instructions, and subjected to rRNA depletion with RiboMinus kit (Ambion). RNA was fragmented to ~100 nucleotide fragments with Ambion fragmentation reagent (40 second incubation at 94°C). 200 ng of RNA was denatured and incubated with 20ul of protein A beads, previously bound to 1 μ g of anti-m⁶A polyclonal antibody (Synaptic Systems) or Rabbit IgG in 1 \times IPP buffer (150 mM NaCl, 10 mM TRIS-HCL and 0.1% NP-40). RNA was incubated with the antibody for 3 hours at 4°C in 1 \times IPP buffer. Beads where washed 2 times with 1 \times IPP buffer, 2 times with low salt buffer (50 mM NaCl, 10 mM TRIS-HCL and 0.1% NP-40), 2 times with high salt buffer (500 mM NaCl, 10 mM TRIS-HCL and 0.1% NP-40) and 1 time with 1 \times IPP buffer. RNA was eluted from the beads with 50 μ l of RLT buffer, and purified with Qiagen RNeasy columns. RNA was eluted in 100 ul of RNase free water.

m⁶A enrichment was analyzed on a LightCycler 480 by RT-qPCR with One-Step RT-PCR Master Mix SYBR Green (Stratagene). The PCR was carried on using a standard protocol with melting curve. The amount of target were calculated using the formula: Amount of target = $2^{-C(T)}$ ³¹. *Myc peak* is positive control, *Myc body* and *Myb* are negative controls for m⁶A RIP qPCR. Two tailed T test for unequal, unpaired data sets with heteroscedastic variation was used to compare samples.

For m⁶A RNA-IP-Seq, we started with 200~300 ug of total RNA from CD4+ T cells isolated from wild type mice using StemCell CD4+ T cell kits. Using the same protocol with scale-

up reagents, the eluted IP RNA were concentrated by ethanol precipitation, and resolved in 10 ul DEPC water. 10 ng RNA from input and enriched IP RNA samples were used for library preparation with the SMARTer Stranded Total RNA-Seq Kit – Pico Input Mammalian (Clontech) according to the manufacturer's instructions. Input and enriched samples were multiplexed with Illumina bar codes and sequenced using paired-end 2×75-nt cycles on an Illumina HiSeq 2500 instrument. To process m⁶A-Seq data, reads were aligned using Tophat2. Macs was then used for peak calling following the protocol in Dominissini et al.³². Samples were normalized to get pileup per million reads in each sample, using the number of reads which were left after filtering redundant tags from MACS³³. Peaks were then visualized using IGV³⁴.

siRNA knockdown

Socs1 siRNA and non-targeting control siRNA were purchased from GE-Dharmacon (E-043120-00-0005), and the experiments were done by strictly following manufacturer's manual. The Naïve T cells with siRNA transfection were incubate in 37°C incubator for 3 hrs, then were transferred into *Rag2*^{-/-} receipt mice by intravenous injection (1 million cells per mice). 4 weeks after transfer, the cells from spleen, peripheral lymph nodes, and mesenteric lymph nodes were analyzed by FACS. Representative FACS images show that the Naïve marker CD45RB peaks shift leftwards upon *Socs1* siRNA treatment.

Mettl3 KO rescue

The WT and catalytic dead *Mettl3* genes were cloned into N103 plasmid in Chang lab. To create a catalytic dead mutant *Mettl3*, we inserted the mutations D395A and W398A (DPPW catalytic motif of METTL3) based on published data, which show that those two residues are absolutely required for METTL3 activity³⁵⁻³⁷. *Mettl3* KO naïve T cells were isolated from *Mettl3* KO mice with StemCell Naïve T cell purification kit, then electroporated by nucleofection by exactly following the Amaxa mouse T cell nucleofector kit manual (Lonza). 4 hours after nucleofection in 37°C incubator, the cells were transferred into *Rag2*^{-/-} receipt mice by intravenous injection (1 million cells per mice). 4 weeks after transfer, the cells from spleen, periphery lymph nodes, and mesenteric lymph nodes were analyzed by FACS for cell numbers, and naïve Cell marker CD45RB. The CD4+ T cells were isolated from lymph nodes using StemCell CD4+ T cell kit, and total RNA was isolated from the CD4+ T cells using Direct-zol RNA microprep columns (Zymo Research). RT-qPCR was performed using the isolated RNAs. Each group has at least 5 mice to ensure statistical significance.

Ribosome Profiling

We performed the Ribosome profiling by strictly following the manual of Illumina TruSeq Ribo Profile (Mammalian) Kit. Briefly, 50 million of Naïve T cells were isolated from WT and *Mettl3* KO mice, and washed and treated with 0.1 mg/ml cycloheximide for 1min. After lysis, 1/10 of the cell lysate were used to isolate RNA for preparing input RNA library, the remaining were used to prepare ribosome footprints by first digested with 60U of 10 U/ul nuclease, then cleaned up by MicroSpin S-400 columns. The total RNAs and ribosome protected RNAs were then isolated with RNA Clean & Concentrator-25 kit (Zymo Research), and subjected to rRNA removal with Illumina Ribo-Zero Gold Kits.

Polyacrylamide gel electrophoresis (PAGE) was used to purify the 28nt and 30nt long ribosome protected fragments, which were ligated 3' adapters and prepared cDNA library. The cDNA library were PAGE gel purified again for the 70–80nt fragments, circularized, and amplified by PCR for 9 cycles, the resulting libraries were cleaned up by AMPure XP beads, purified by PAGE purification for 140~160bp fragments, and subjected to Illumina Hi-Seq for 75bp paired-end sequencing.

We used the tuxedo suite (<https://ccb.jhu.edu/software/tophat/>) to align the ribosome profiling reads and determine FPKM, fold change, and the associated p-value. All genes which did not have enough reads aligned to determine FPKM were discarded, and the remaining genes were plotted. To calculate translation efficiency, HTseq was used to count the number of reads in each experiment. The normalized translation efficiency was calculated by taking the log₂ of the quotient of the ribosome footprint read count divided by the mRNA-Seq read count. The individual graphs were plotted using R package (<https://bioconductor.org/packages/release/bioc/html/Sushi.html>).

Enrichment of s4U-labeled RNA

Naïve T cells were isolated from *Mettl3* KO and WT mice with Naïve T cell purification kits (StemCell). The cells were counted and aliquoted 4million per 1mL FACS buffer per Eppendorf tube. Each tube except t=0 receives 10 µg/ml IL-7 cytokine and incubate in 37°C incubator. 15minu before spanned down and lysed with Trizol, the cells were labeled with 250 µM s4U. The Enrichment of s4U-RNA was performed using MTS-biotin chemistry^{23,38}. Briefly, cells were lysed in TRIzol, extracted with chloroform once and the nucleic acids precipitated with isopropanol. DNA was removed with DNase, the proteins removed with phenol:chloroform:isoamylalcohol extraction, and RNA isolated using isopropanol precipitation. Total RNA was sheared to ~200bp by adding shearing buffer (150 mM Tris-HCl, pH 8.3, 225 mM KCl, 9 mM MgCl₂) and heating to 94°C for 4 min, followed by quench on ice with EDTA. Sheared RNA was purified using a modified protocol with the RNeasy Mini Kit (Qiagen). To biotinylate the s4U-RNA, 20 µg sheared RNA was incubated with 2 µg MTS-biotin in biotinylation buffer for 30 min. Excess biotin was removed via chloroform extraction using Phase-Lock Gel Tubes. RNA was precipitated with a 1:10 volume of 3 M NaOAc and an equal volume of isopropanol and centrifuged at 20,000 × g for 20 min. The pellet was washed with an equal volume of 75% ethanol. Purified RNA was dissolved in 50 µL RNase-free water. Biotinylated RNA was separated from non-labeled RNA using glycogen-blocked Dynabeads Streptavidin C1 Beads (Invitrogen). Beads (10 µL) were added to each sample and incubated for 15 min at room temperature, then washed three times with high salt wash buffer (100 µL each, 100 mM Tris-HCl [pH 7.4], 10mM EDTA, 1 M NaCl, and 0.1% Tween-20). In order to improve the stringency of the washes, an additional 3 washes with buffer TE (10 mM Tris pH 7.4, 1 mM EDTA) at 55°C were added to the protocol. s4U-RNA was eluted from Dynabeads with 25 µL freshly prepared elution buffer (10 mM DTT, 100 mM NaCl, 10 mM Tris pH 7.4, 1 mM EDTA, 10 pg/µL *S. pombe* total RNA [a generous gift from Julien Berro]) and incubated for 15 min, followed by a second elution with an additional 25µL elution buffer. Both elutions were pooled and purified by ethanol precipitation. 1% input (200ng sheared RNA) was also saved from each

sample before enrichment, and 500pg *S. pombe* total RNA was added as a normalization spike-in.

s4U-Seq library preparation and sequencing

10ng RNA from input and enriched RNA samples was used for library preparation with the SMARTer Stranded Total RNA-Seq Kit – Pico Input Mammalian (Clontech) according to the manufacturer's instructions. Input and enriched samples were multiplexed with Illumina bar codes and sequenced using single-end 1×75-nt cycles on an Illumina HiSeq instrument.

Mapping and quantification of s4U-Seq libraries

Sequencing reads were aligned using STAR (version 2.4.2a; Dobin 2013) to a joint index of the *M. musculus* and *S. pombe* genomes (mm10 and sp2) and transcriptomes (UCSC and Ensembl Fungi v22)^{39,40}. Alignments and analysis were performed on the Yale High Performance Computing clusters. Following alignment, HTSeq-count (version 0.6.1p1) was used to quantify annotated *M. musculus* and *S. pombe* transcripts for total RNA (–t gene) and mRNA (–t exon)⁴¹. Tracks normalized using the *S. pombe* reads were uploaded to the UCSC genome browser. The scale was normalized using exogenous *S. pombe* RNA added prior to library preparation.

Transcript abundance, synthesis and degradation rates were estimated using the INSPEcT package in R⁴². Spearman correlation between samples were visualized using the corrplot package. Transcripts with significant time-dependent changes were determined and clustered using the maSigPro package in R and heatmaps were made using the pheatmap package⁴³.

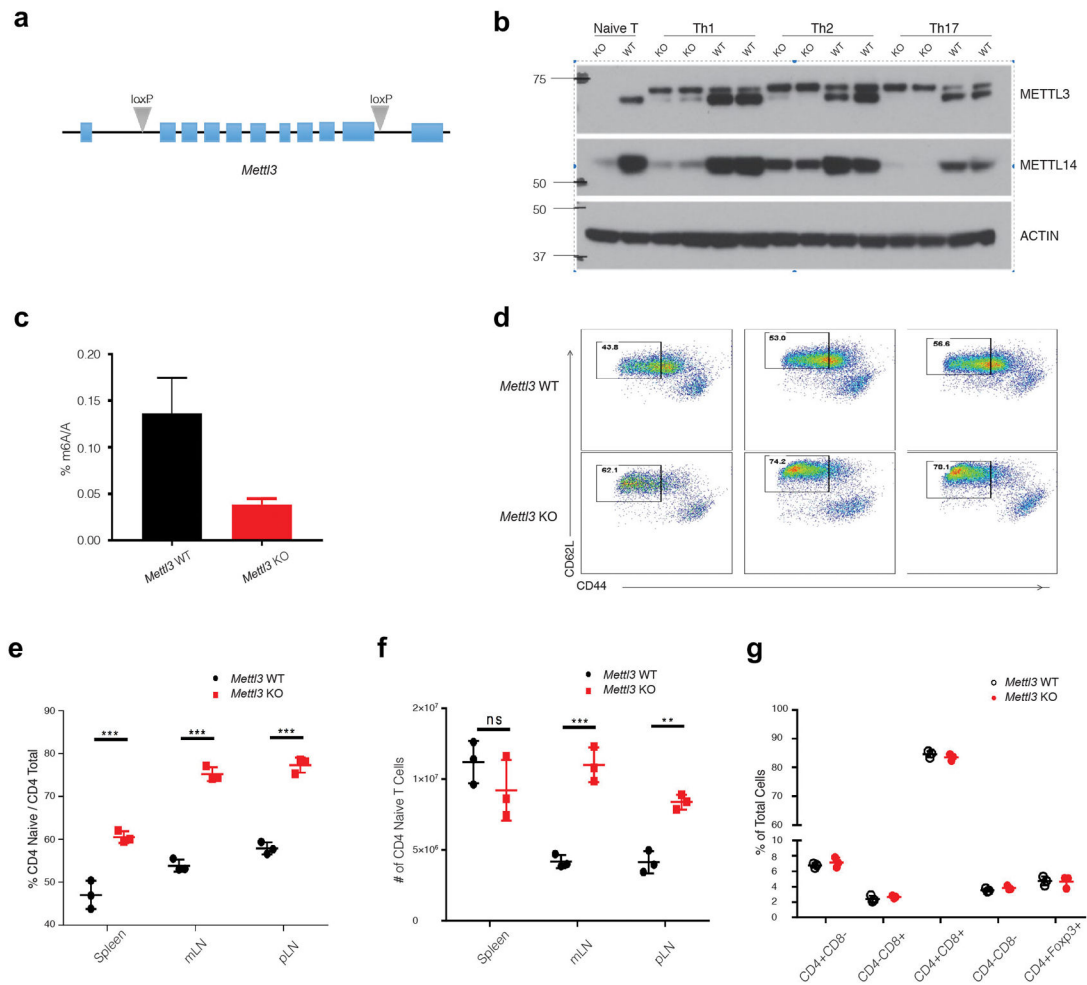
Statistical Analysis

The sample size chosen for our animal experiments in this study was estimated based on our prior experience of performing similar sets of experiments. All animal results were included and no method of randomization was applied. We at least independently repeated the data once, and all attempt to reproduce the results were successful. For all the bar graphs, data were expressed as mean ± SEM. Statistical analyses were performed using GraphPad Prism 6. Differences were analyzed by Student's t test, or Two-way ANOVA test using GraphPad Prism 6. P values < 0.05 were considered significant (*: $P < 0.05$; **: $P < 0.001$; ***: $P < 0.0001$); P values >0.05; non-significant (NS). FlowJo (Treestar) was used to analyze all the flow cytometry data. The sample sizes (biological replicates), specific statistical tests used, and the main effects of our statistical analyses for each experiment were detailed in each figure legend.

Data Availability Statement

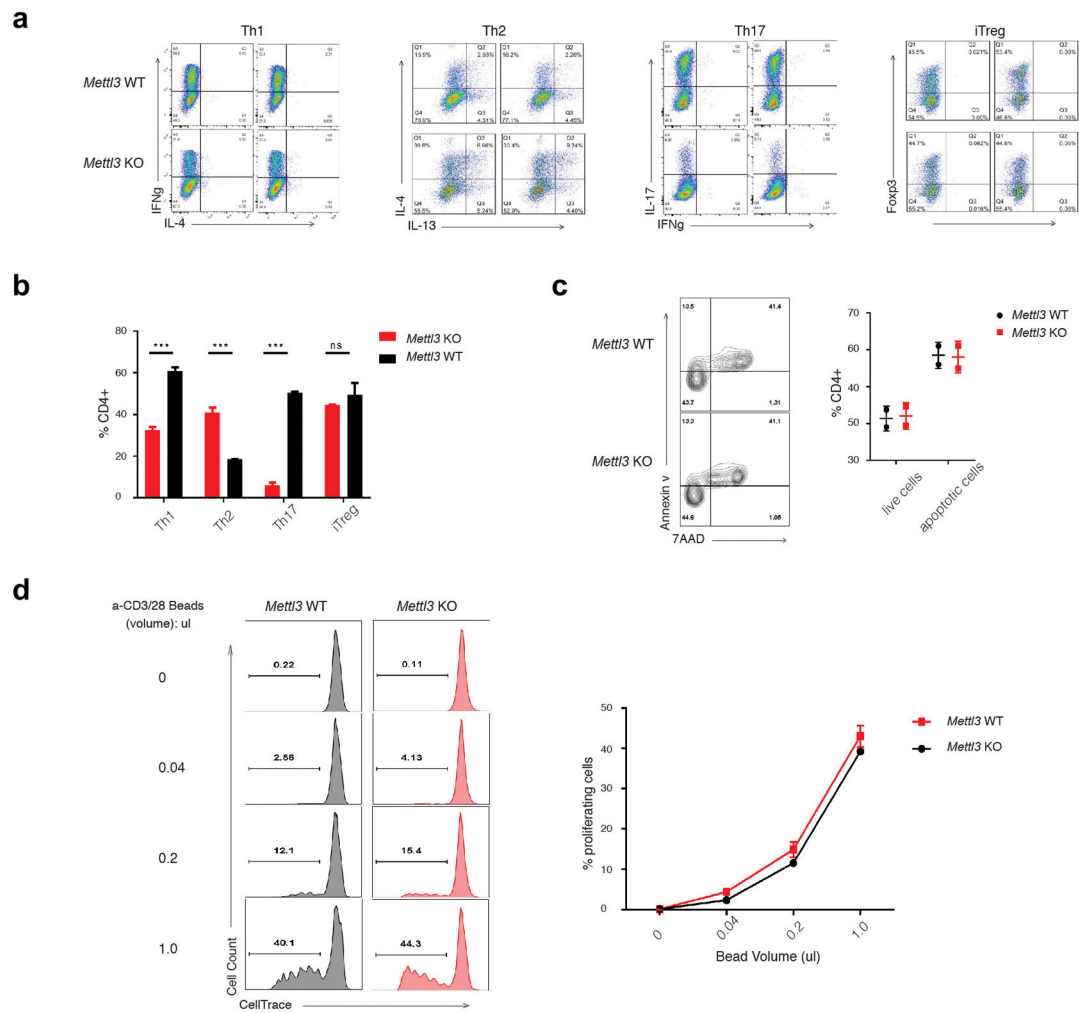
The data that support the findings of this study are available from the corresponding author upon reasonable request. RNA-Seq, Ribosome Profiling, s4U-Seq, and m⁶A RIP-Seq datasets have been deposited in GEO under the accession number: GSE100048.

Extended Data



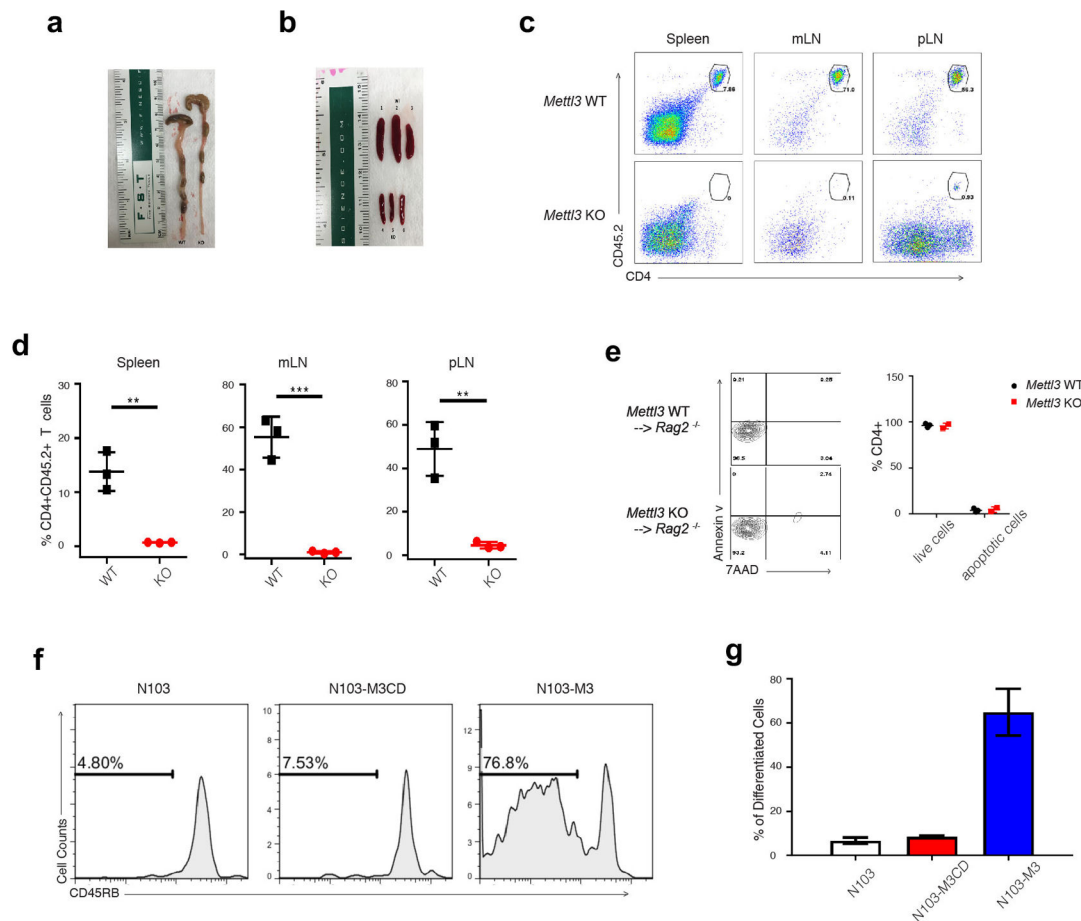
Extended Data Figure 1. Abnormal T cell homeostasis in generated *Mettl3* CD4-CRE conditional Knockout mice

a, The two lox sites were inserted into the first and last introns by CRISPR technology. **b**, Protein levels of METTL3 and its associated METTL14 were analyzed by Western Blot in the naïve T cells and in vitro differentiated Th1, Th2, Th17 cells from *Mettl3* KO and WT mice. **c**, Overall levels of RNA m⁶A methylation in Naïve T cells from *Mettl3* KO and WT mice. **d**, Naïve T cells increased in all lymphoid organs from *Mettl3* KO mice comparing to littermate control WT mice. Cells from spleen (SPL), mesenteric lymph node (mLN), and peripheral lymph node (pLN) were analyzed by FACS by staining with CD4/CD44/CD62L. **e**, The percentage of CD4+CD44^{low}CD62⁺ naïve T cells increased in all three lymphoid organs in *Mettl3* KO mice, **f**, and the total number of naïve T cells in mLN and pLN also increased in KO mice. **g**, The cell population in the thymus do not have any changes in *Mettl3* KO.



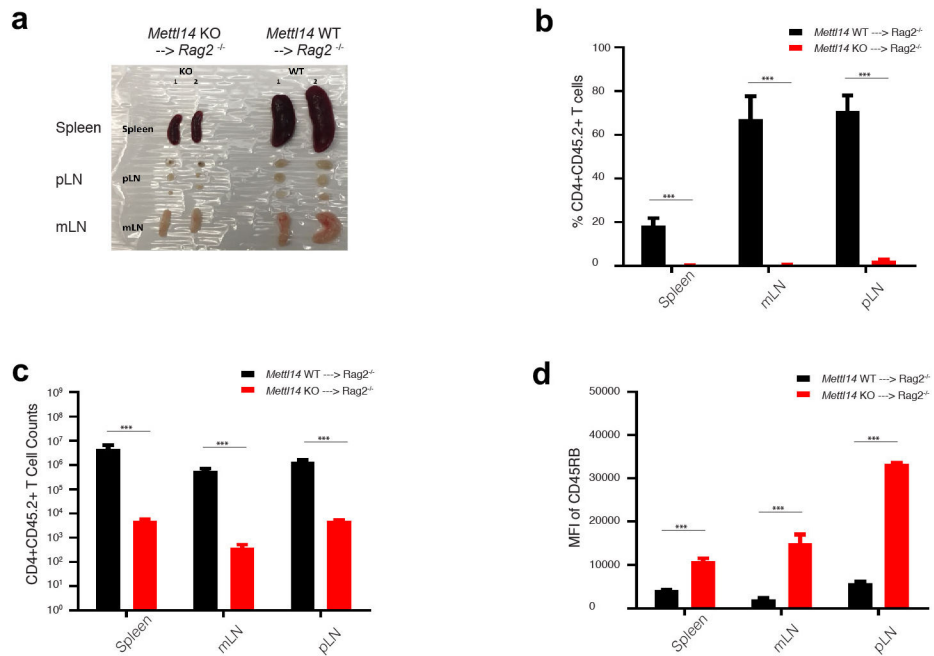
Extended Data Figure 2. Naïve T cells from *Mettl3* KO mice differentiated into less Th1 and Th17 cells, more Th2 cells *ex vivo* comparing to WT naïve T cells

a, Naïve T cells isolated from *Mettl3* WT and KO mice were differentiated into effector subsets under defined optimal conditions. **b**, The percentages of each T cell subtypes over total CD4⁺ T cells were analyzed by FACS. **c**, No apoptosis defects were found in *ex vivo* cultured cells from WT and *Mettl3* KO naïve T cells by FACS staining of Annexin V and 7AAD. Double negative stained cells are live cells, and the remaining are apoptotic cells. The percentage is listed in the right graph. **d**, No proliferation differences were found in *ex vivo* cultured cells from WT and *Mettl3* KO naïve T cells. Naïve T cells labeled with CellTrace were culture *ex vivo* under different concentration of Anti-CD3/CD28 beads for 4 days. The percentages of proliferating cells were listed in the right graph.

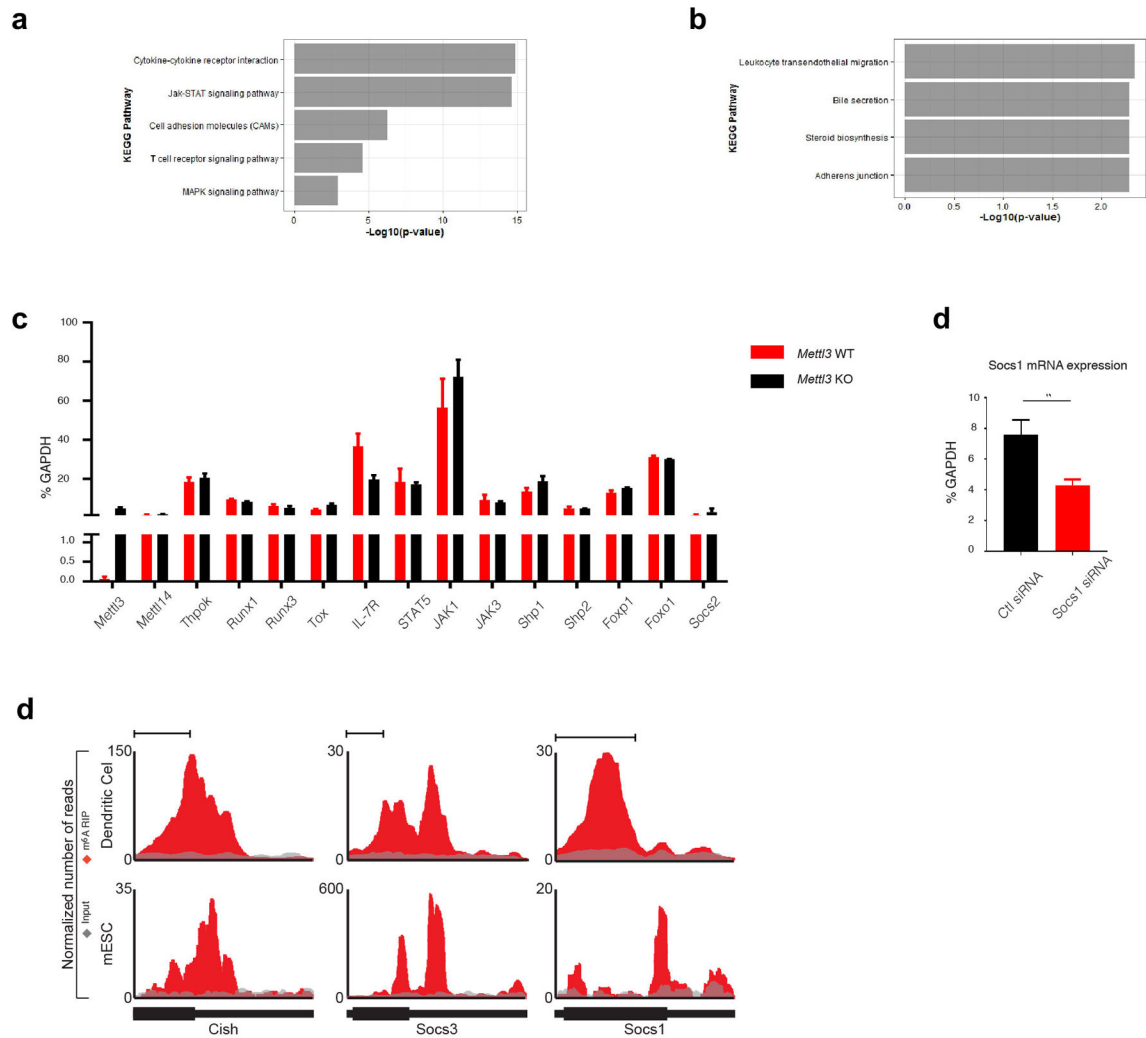


Extended Data Figure 3. m⁶A methylation function of *Mettl3* controls Naïve T cell homeostatic expansion

a, *Mettl3*^{-/-} receipts had normal colon length, and *Mettl3*^{+/+} receipts had shorter colon length. **b**, *Mettl3*^{+/+} receipts had enlarged spleens indicative of normal homeostatic expansion, while *Mettl3*^{-/-} receipts have very small spleens. **c**, All lymph organs have much less transferred KO cells comparing to WT cells analyzed by FACS. **d**, the percentage of transferred *Mettl3* KO and WT cells in *Rag2*^{-/-} host mice. **e**, No apoptosis defects were found in *in vivo* cells recovered from peripheral lymph nodes of *Mettl3* WT and KO receipt mice by FACS staining of Annexin V and 7AAD. Double negative stained cells are live cells, and the remaining are apoptotic cells. The percentage is listed in the right graph. **f-g**, WT *Mettl3* constructs, but not m⁶A catalytic dead *Mettl3* constructs, could rescue *Mettl3* KO *in vivo* defect phenotypes. Empty construct (N103), catalytic dead *Mettl3* construct (N103-CD), and WT *Mettl3* construct (N103-M3) were electroporated into *Mettl3* KO Naïve T cells, and then transferred into *Rag2*^{-/-} mice. Four weeks after transfer, the cell number (proliferation) and CD45RB marker (differentiation) were analyzed by FACS, and representative images were shown in **f**, and the statistics of cell number were shown in **g**.

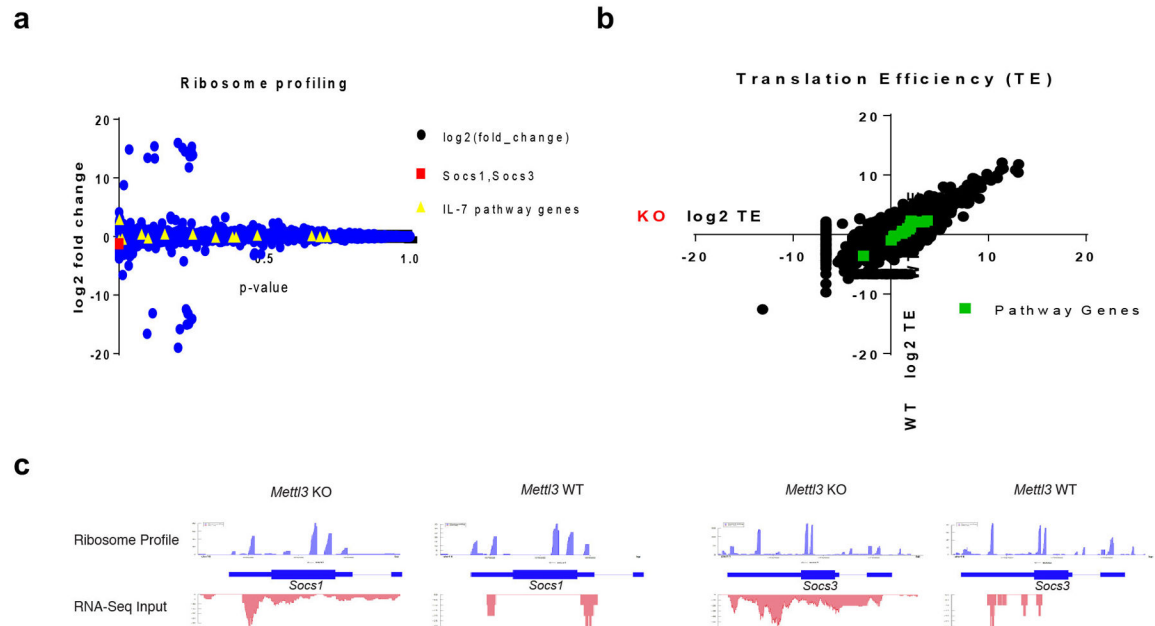


Extended Data Figure 4. *Mettl14* KO naïve T cell adoptive transfer phenocopies *Mettl3* KO cells
a, *Mettl14* KO receipt mice have smaller lymphoid organs, including spleen, peripheral lymph nodes, and mesenteric lymph nodes. **b–c**, The percentage and the number of transferred *Mettl14* KO cells in *Rag2*^{-/-} receipt mice were much less than that of WT cells 4 weeks after transfer in all lymphoid organs. **d**, The MFI (Median Fluorescence Intensity) of naïve marker CD45RB is much higher in KO than WT, suggesting *Mettl14* naïve T cells were locked in naïve state while WT naïve T cells differentiated after 4 weeks in *Rag2*^{-/-} mice.



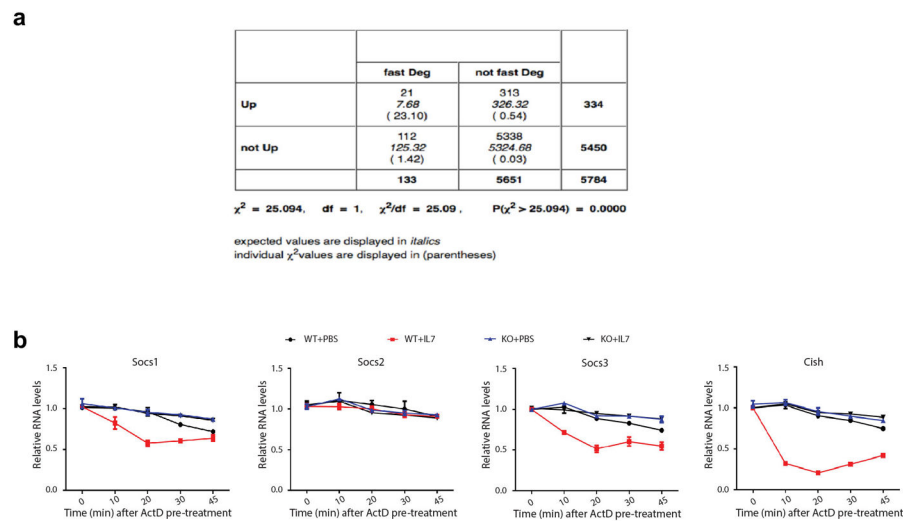
Extended Data Figure 5. Socs genes are the m⁶A targets that contribute to the observed phenotypes

a, Up-regulated KEGG pathways in *Mettl3* KO cells over WT cells based on RNA-Seq data. **b**, Down-regulated pathways in *Mettl3* KO cells over WT cells. **c**, RT-qPCR validated the RNA-Seq data that the mRNA expression levels of other genes and regulators in IL-7 pathways did not change in *Mettl3* KO naïve T cells comparing to WT cells (n=6). **d**, *Socs1* siRNAs knock down *Socs1* gene expression by half in vitro. Naïve T cells were incubated with *Socs1* or control siRNA *in vitro* for 3 days, and RT-qPCR was used to measure the mRNA levels of *Socs1* gene. **e**, *Socs1*, *Socs3* and *Cish* mRNA 3' UTRs are enriched with m⁶A peaks from published ESC and Dendritic Cell m⁶A-RIP genome mapping. Red denotes the IP RNA counts, and Grey denotes input.



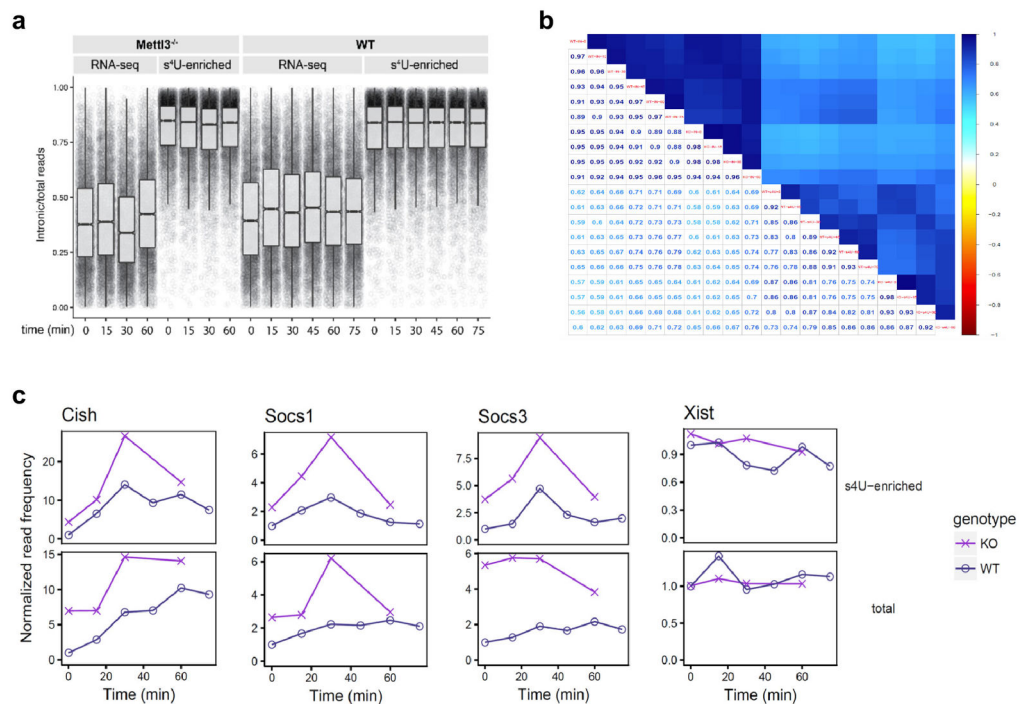
Extended Data Figure 6. Ribosome profiling does not reveal any ribosome occupancy differences in IL-7 and TCR signaling related genes

a. Overall statistical analysis for all genes. *Socs* genes and other IL-7 pathway genes are highlighted. The y-axis is the log (base2) fold change of *Mettl3* KO over WT, and the x-axis plots the p-value of the fold change value. **b.** Calculated translation efficiency for all genes, and the IL-7 & TCR pathway genes do not show difference in translation efficiency between *Mettl3* KO and WT naïve T cells. **c.** Overall levels of RNA m⁶A methylation in Naïve T cells from *Mettl3* KO and WT mice. **c-d.** Example ribosome profiles of *Socs1* and *Socs3* mRNAs, which do not show any significant differences between WT (right panel) and *Mettl3* KO (left panel) samples. The RNA-Seq for the inputs are shown below the ribosome profiles, which also demonstrate enhanced mRNA expression for *Socs* genes.



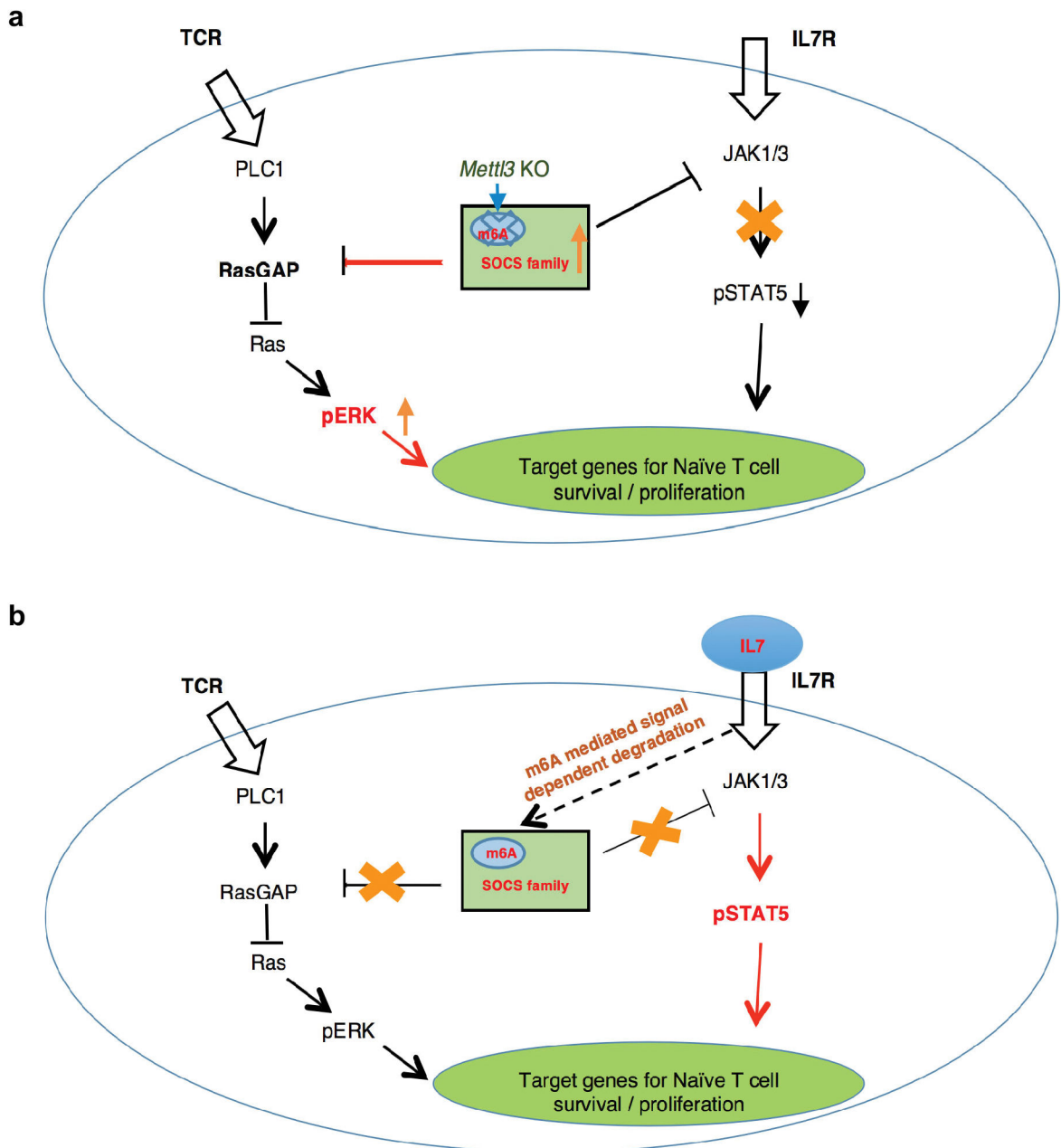
Extended Data Figure 7. Socs genes are signal inducible degradation-controlled genes

a, Up-regulated genes in *Mettl3* KO Naïve T cells are significantly enriched in the degradation-controlled group of genes from LPS stimulated dendritic cells. We compared the genes differentially regulated by m⁶A in naïve T cells to degradation controlled genes in dendritic cells. We can assign cluster information to 5784 genes in our sequencing dataset. Looking at the clusters where fast degradation plays a key role (cluster 2, 4 and 6), and asking if the number of genes unregulated is significant, with a chi square test. The p value is < 0.0001. fast deg --- genes in clusters 2,5,6; not fast deg --- all other clusters; Up --- genes unregulated (marked as significant and positive fold change); Not up --- genes that don't change or are down-regulated. **b**, *Socs1*, *Socs3*, and *Cish*, but not *Socs2* degrade faster upon IL-7 treatment in WT cells, and the faster degradation with IL-7 stimulation is abrogated in *Mettl3* KO naïve T cells. The Naïve T cells isolated from both WT or *Mettl3* KO mice were pre-treated with Actinomycin-D for 1hr to fully stop transcription before IL-7 stimulation, the residual mRNAs at different time points were normalized back to t=0 (100%).



Extended Data Figure 8. Summary of s4U-Seq data

a, Analysis of reads mapping to introns demonstrates high intronic read density in s4U-enriched samples. The ratio of reads mapping to introns is expressed as a ratio to the total number of reads that map to each transcript in each sample. **b**, Plot illustrating the Spearman correlations of the transcript-level read frequencies in total and s4U-enriched samples for WT and *Mettl3* KO cells at various times after IL-7 stimulation. **c**, Changes in transcript frequencies after IL-7 stimulation for WT or *Mettl3* KO cells with and without s4U enrichment based on s4U-Seq data. Expression levels are presented relative to the transcript levels of WT cells before IL-7 stimulation. Shown are cluster-3 Socs genes and a control gene *Xist*.



Extended Data Figure 9. Working model for m⁶A controlled Naïve T cell homeostasis
a, *Mettl3* KO Naïve T cell molecular Mechanism: Loss of m⁶A lead to slower Socs mRNA degradation and increased SOCS protein levels, which blocked the IL7 pathway. **b**, Revised T cell differentiation model: m⁶A targets *Socs1*, *Socs3* and *Cish* for inducible and rapid mRNA degradation upon IL-7 stimulation, allowing IL-7-JAKs signaling to activate the downstream target STAT5, to initiate the re-programming of the naïve T cells for differentiation and proliferation.

Supplementary Material

Refer to Web version on PubMed Central for supplementary material.

Acknowledgments

We thank R. Flynn, R. Jackson, Y. Yang, M. Vesely, R. Paiva, N. Palm and all the other members of the Flavell lab for discussions and comments. We thank J. Alderman, C. Lieber, C. Hughes and J. Stein for technical support. H.-B.L. was supported by NIH T32 2T32DK007356. S.Z was supported by the fellowship from Helen Hay Whitney Foundation-Howard Hughes Medical Institute. This work was supported by the Howard Hughes Medical Institute (R.A.F.), R01-HG004361 (H.Y.C.), NIH New Innovator Award DP2 HD083992-01 (M.D.S.), and a Searle scholarship (M.D.S.).

References

1. Cao G, Li HB, Yin Z, Flavell RA. Recent advances in dynamic m6A RNA modification. *Open Biol.* 2016; 6:160003. [PubMed: 27249342]
2. Fu Y, Dominissini D, Rechavi G, He C. Gene expression regulation mediated through reversible m(6)A RNA methylation. *Nature reviews. Genetics.* 2014; 15:293–306. DOI: 10.1038/nrg3724
3. Geula S, et al. Stem cells. m6A mRNA methylation facilitates resolution of naive pluripotency toward differentiation. *Science.* 2015; 347:1002–1006. DOI: 10.1126/science.1261417 [PubMed: 25569111]
4. Batista PJ, et al. m(6)A RNA Modification Controls Cell Fate Transition in Mammalian Embryonic Stem Cells. *Cell stem cell.* 2014; 15:707–719. DOI: 10.1016/j.stem.2014.09.019 [PubMed: 25456834]
5. Collins A, Littman DR. Selection and lineage specification in the thymus: commitment 4-stalled. *Immunity.* 2005; 23:4–5. DOI: 10.1016/j.immuni.2005.07.003 [PubMed: 16039574]
6. Esplugues E, et al. Control of TH17 cells occurs in the small intestine. *Nature.* 2011; 475:514–518. DOI: 10.1038/nature10228 [PubMed: 21765430]
7. Ostanin DV, et al. T cell transfer model of chronic colitis: concepts, considerations, and tricks of the trade. *American Journal of Physiology-Gastrointestinal and Liver Physiology.* 2009; 296:G135–G146. DOI: 10.1152/ajpgi.90462.2008 [PubMed: 19033538]
8. Martin CE, Frimpong-Boateng K, Spasova DS, Stone JC, Surh CD. Homeostatic proliferation of mature T cells. *Methods in molecular biology.* 2013; 979:81–106. DOI: 10.1007/978-1-62703-290-2_9 [PubMed: 23397391]
9. Takada K, Jameson SC. Naive T cell homeostasis: from awareness of space to a sense of place. *Nature reviews. Immunology.* 2009; 9:823–832. DOI: 10.1038/nri2657
10. Sprent J, Surh CD. Normal T cell homeostasis: the conversion of naive cells into memory-phenotype cells. *Nature immunology.* 2011; 12:478–484. DOI: 10.1038/ni.2018 [PubMed: 21739670]
11. Yoshimura A, Naka T, Kubo M. SOCS proteins, cytokine signalling and immune regulation. *Nature Reviews Immunology.* 2007; 7:454–465. DOI: 10.1038/nri2093
12. Palmer DC, Restifo NP. Suppressors of cytokine signaling (SOCS) in T cell differentiation, maturation, and function. *Trends in immunology.* 2009; 30:592–602. DOI: 10.1016/j.it.2009.09.009 [PubMed: 19879803]
13. Surh CD, Sprent J. Homeostasis of Naive and Memory T Cells. *Immunity.* 2008; 29:848–862. DOI: 10.1016/j.immuni.2008.11.002 [PubMed: 19100699]
14. Chong MM, et al. Suppressor of cytokine signaling-1 is a critical regulator of interleukin-7-dependent CD8+ T cell differentiation. *Immunity.* 2003; 18:475–487. [PubMed: 12705851]
15. Cacalano NA, Sanden D, Johnston JA. Tyrosine-phosphorylated SOCS-3 inhibits STAT activation but binds to p120 RasGAP and activates Ras. *Nature cell biology.* 2001; 3:460–465. DOI: 10.1038/35074525 [PubMed: 11331873]

16. Matsumoto A, et al. A role of suppressor of cytokine signaling 3 (SOCS3/CIS3/SSI3) in CD28-mediated interleukin 2 production. *The Journal of experimental medicine*. 2003; 197:425–436. [PubMed: 12591901]
17. Matsumoto A, et al. Suppression of STAT5 functions in liver, mammary glands, and T cells in cytokine-inducible SH2-containing protein 1 transgenic mice. *Mol Cell Biol*. 1999; 19:6396–6407. [PubMed: 10454585]
18. Yue Y, Liu J, He C. RNA N6-methyladenosine methylation in post-transcriptional gene expression regulation. *Genes & development*. 2015; 29:1343–1355. DOI: 10.1101/gad.262766.115 [PubMed: 26159994]
19. Schwartz S, et al. Perturbation of m6A Writers Reveals Two Distinct Classes of mRNA Methylation at Internal and 5' Sites. *Cell reports*. 2014; 8:284–296. DOI: 10.1016/j.celrep.2014.05.048 [PubMed: 24981863]
20. Tani H, Akimitsu N. Genome-wide technology for determining RNA stability in mammalian cells: historical perspective and recent advantages based on modified nucleotide labeling. *RNA biology*. 2012; 9:1233–1238. DOI: 10.4161/rna.22036 [PubMed: 23034600]
21. Rabani M, et al. Metabolic labeling of RNA uncovers principles of RNA production and degradation dynamics in mammalian cells. *Nat Biotech*. 2011; 29:436–442. DOI: 10.1038/nbt.1861
22. Rabani M, et al. High-Resolution Sequencing and Modeling Identifies Distinct Dynamic RNA Regulatory Strategies. *Cell*. 2014; 159:1698–1710. doi:<http://dx.doi.org/10.1016/j.cell.2014.11.015>. [PubMed: 25497548]
23. Duffy EE, et al. Tracking Distinct RNA Populations Using Efficient and Reversible Covalent Chemistry. *Molecular cell*. 2015; 59:858–866. DOI: 10.1016/j.molcel.2015.07.023 [PubMed: 26340425]
24. Henao-Mejia J, et al. Generation of Genetically Modified Mice Using the CRISPR-Cas9 Genome-Editing System. *Cold Spring Harb Protoc*. 2016 pdb prot090704.
25. Gagliani N, et al. TH17 cells transdifferentiate into regulatory T cells during resolution of inflammation. *Nature*. 2015; 523:221–U225. DOI: 10.1038/nature14452 [PubMed: 25924064]
26. Kim D, et al. TopHat2: accurate alignment of transcriptomes in the presence of insertions, deletions and gene fusions. *Genome biology*. 2013; 14:R36. [PubMed: 23618408]
27. Trapnell C, et al. Transcript assembly and quantification by RNA-Seq reveals unannotated transcripts and isoform switching during cell differentiation. *Nature biotechnology*. 2010; 28:511–U174. DOI: 10.1038/nbt.1621
28. Wang J, Duncan D, Shi Z, Zhang B. WEB-based GENE SeT AnaLysis Toolkit (WebGestalt): update 2013. *Nucleic acids research*. 2013; 41:W77–W83. DOI: 10.1093/nar/gkt439 [PubMed: 23703215]
29. Wickham H. ggplot2: Elegant Graphics for Data Analysis. *Use R*. 2009:1–212. DOI: 10.1007/978-0-387-98141-3
30. Shen S, et al. rMATS: robust and flexible detection of differential alternative splicing from replicate RNA-Seq data. *Proceedings of the National Academy of Sciences of the United States of America*. 2014; 111:E5593–5601. DOI: 10.1073/pnas.1419161111 [PubMed: 25480548]
31. Livak KJ, Schmittgen TD. Analysis of relative gene expression data using real-time quantitative PCR and the 2^{(-Delta Delta C(T))} Method. *Methods*. 2001; 25:402–408. DOI: 10.1006/meth.2001.1262 [PubMed: 11846609]
32. Dominissini D, Moshitch-Moshkovitz S, Salmon-Divon M, Amariglio N, Rechavi G. Transcriptome-wide mapping of N(6)-methyladenosine by m(6)A-seq based on immunocapturing and massively parallel sequencing. *Nature protocols*. 2013; 8:176–189. DOI: 10.1038/nprot.2012.148 [PubMed: 23288318]
33. Zhang Y, et al. Model-based analysis of ChIP-Seq (MACS). *Genome biology*. 2008; 9:R137. [PubMed: 18798982]
34. Robinson JT, et al. Integrative genomics viewer. *Nature biotechnology*. 2011; 29:24–26. DOI: 10.1038/nbt.1754
35. Sledz P, Jinek M. Structural insights into the molecular mechanism of the m(6)A writer complex. *eLife*. 2016; 5

36. Clancy MJ, Shambaugh ME, Timpte CS, Bokar JA. Induction of sporulation in *Saccharomyces cerevisiae* leads to the formation of N6-methyladenosine in mRNA: a potential mechanism for the activity of the IME4 gene. *Nucleic acids research*. 2002; 30:4509–4518. [PubMed: 12384598]
37. Wang P, Doxtader KA, Nam Y. Structural Basis for Cooperative Function of Mettl3 and Mettl14 Methyltransferases. *Molecular cell*. 2016; 63:306–317. DOI: 10.1016/j.molcel.2016.05.041 [PubMed: 27373337]
38. Duffy EE, Simon MD. Enriching s4 U-RNA Using Methane Thiosulfonate (MTS) Chemistry. *Curr Protoc Chem Biol*. 2016; 8:234–250. DOI: 10.1002/cpch.12 [PubMed: 27925666]
39. Rosenbloom KR, et al. The UCSC Genome Browser database: 2015 update. *Nucleic acids research*. 2015; 43:D670–681. DOI: 10.1093/nar/gku1177 [PubMed: 25428374]
40. Kersey PJ, et al. Ensembl Genomes: an integrative resource for genome-scale data from non-vertebrate species. *Nucleic acids research*. 2012; 40:D91–97. DOI: 10.1093/nar/gkr895 [PubMed: 22067447]
41. Anders S, Pyl PT, Huber W. HTSeq--a Python framework to work with high-throughput sequencing data. *Bioinformatics*. 2015; 31:166–169. DOI: 10.1093/bioinformatics/btu638 [PubMed: 25260700]
42. de Pretis S, et al. INSPEcT: a computational tool to infer mRNA synthesis, processing and degradation dynamics from RNA- and 4sU-seq time course experiments. *Bioinformatics*. 2015; 31:2829–2835. DOI: 10.1093/bioinformatics/btv288 [PubMed: 25957348]
43. Nueda MJ, Tarazona S, Conesa A. Next maSigPro: updating maSigPro bioconductor package for RNA-seq time series. *Bioinformatics*. 2014; 30:2598–2602. DOI: 10.1093/bioinformatics/btu333 [PubMed: 24894503]

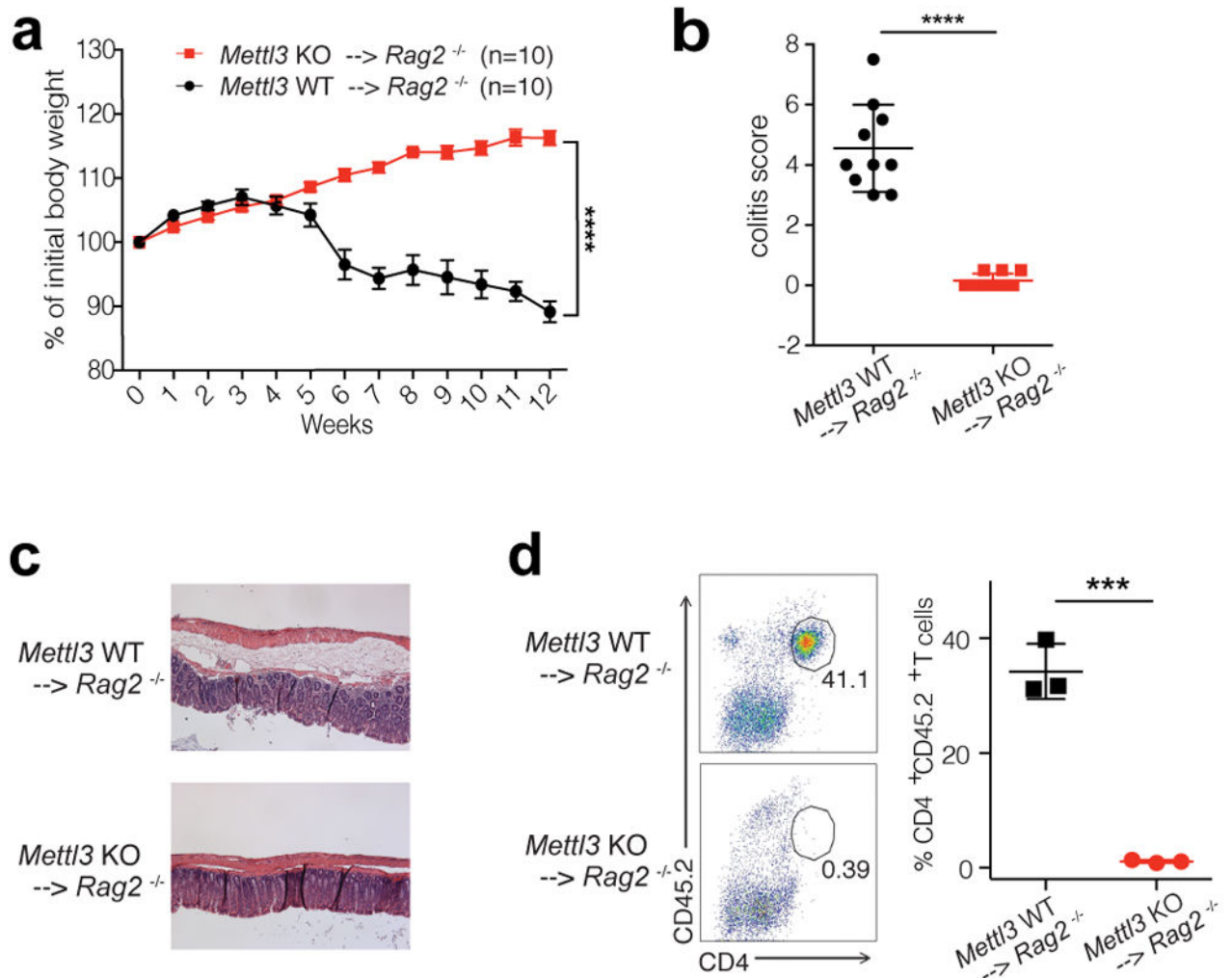


Figure 1. *Mettl3* KO naïve T cells do not promote disease in CD45RB-High adoptive transfer colitis mouse model

a, Body weight changes after naïve T cell adoptive transfer into *Rag2*^{-/-} host mice (n=10), 2-way ANOVA. **b**, **c**, Endoscopic colitis scores and representative pictures of H&E staining of the colon from *Rag2*^{-/-} receiving WT and KO naïve T cells 8 weeks after transfer (n=10), unpaired t test. **d**, FACS analysis of transferred T cells in colon tissues (n=3), unpaired t test. n=number of biological replicates. p***<0.001, p****<0.0001.

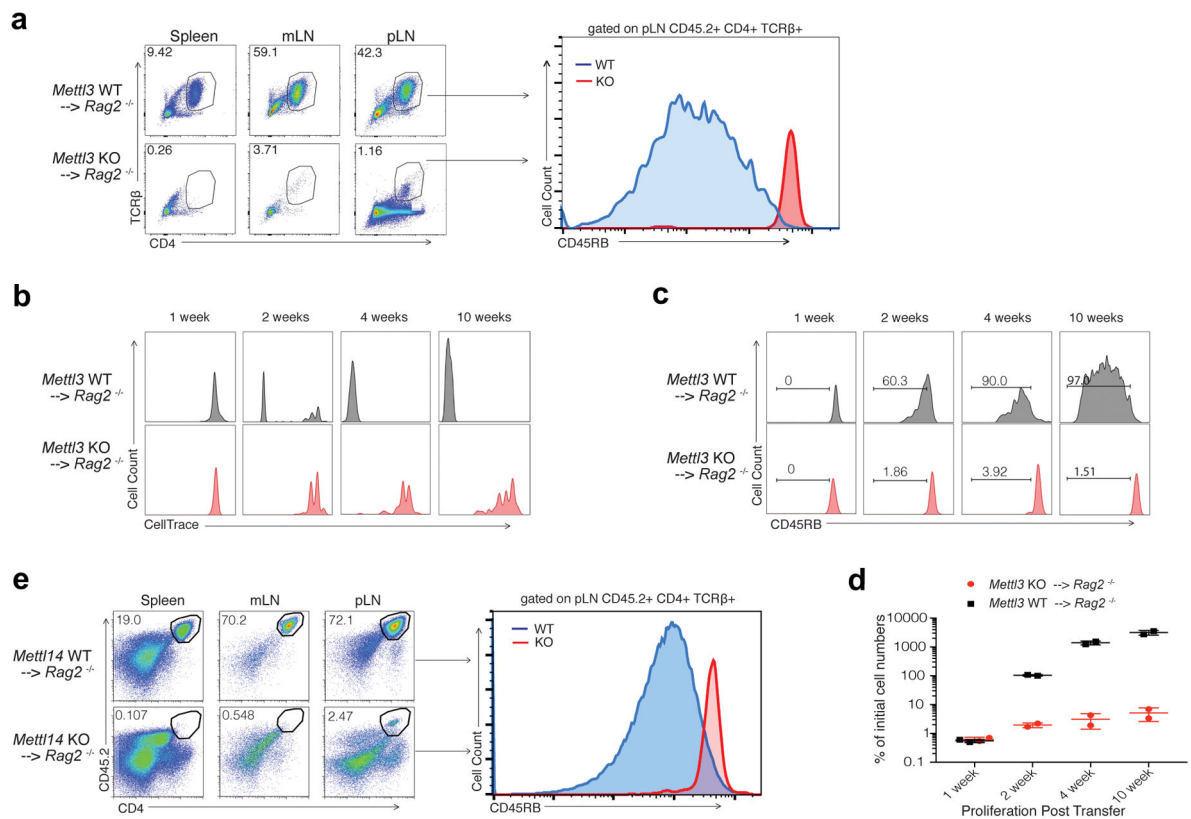


Figure 2. *Mettl3* KO naïve T cells are locked in the naïve state and proliferate much slower than WT cells after transfer into *Rag2*^{-/-} mice

a, Most of the *Mettl3* KO donor cells are retained in lymph nodes (LN) and are locked in naïve states 12 weeks after transfer. **b**, The WT donor naïve T cells start to differentiate from the second week after transfer (CD45RB^{low}), while the *Mettl3* KO donor naïve T cells always stay in naïve states (CD45RB^{high}). **c, d**, The WT donor naïve T cells are driven to proliferate rapidly from the 2nd week, while the *Mettl3* KO T cells slowly proliferate, with the total number of cells recovered from pLN shown in (**d**). **e**, *Mettl14* KO donor naïve T cells recapitulate the phenotype of *Mettl3* KO donor cells. At least 6 animals in each group were analyzed, and representative images were shown.

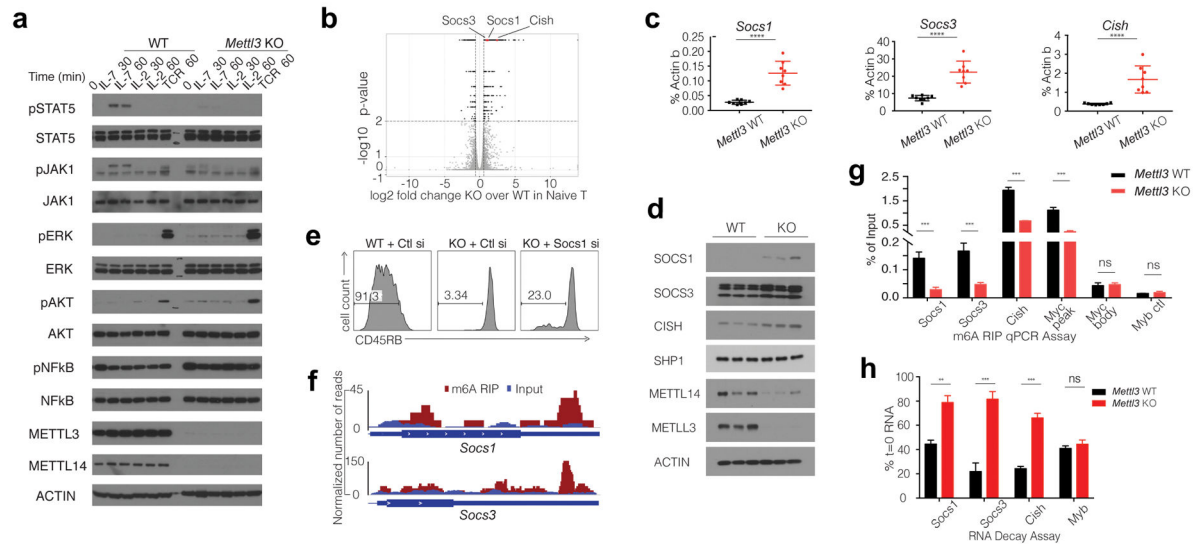


Figure 3. Overexpressed m⁶A target genes *Socs1*, *Socs3* and *Cish* in *Mettl3* KO naïve T cells suppress IL-7/STAT5 signaling pathway

a, Phosphorylation of STAT5 and JAK1 is diminished upon IL-7 stimulation *in vitro*, and basal levels of ERK and AKT phosphorylation are enhanced in KO naïve T cells. **b**, *Socs1*, *Socs3* and *Cish* are among the most significant up-regulated genes in *Mettl3* KO over WT naïve T cells from RNA-Seq. **c**, **d**, RT-qPCR and Western Blots validate that *Socs1*, *Socs3* and *Cish* mRNA are over-expressed in *Mettl3* KO versus WT naïve T cells, unpaired t test. **e**, *Socs1* siRNA knockdown in *Mettl3* KO naïve T cells partially rescues the differentiation defects 4 weeks after transfer into *Rag2*^{-/-} mice. **f**, m⁶A peaks are enriched in 3'-UTR of *Socs1* and *Socs3* genes from m⁶A RIP-Seq data with WT CD4⁺ T cells. **g**, *Socs1*, *Socs3* and *Cish* are m⁶A modified, and the marker is lost in *Mettl3* KO naïve T cells., 2-way ANOVA. **h**, RNA degradation assay shows *Socs1*, *Socs3* and *Cish* mRNAs degrade slower in *Mettl3* KO naïve T cells than that in WT cells two hours after Actinomycin-D treatment. The residual RNA were normalized to t=0. Three independent experiments were done for all the blots and qPCR assays. **p<0.01. ***p<0.001. ****p<0.0001.

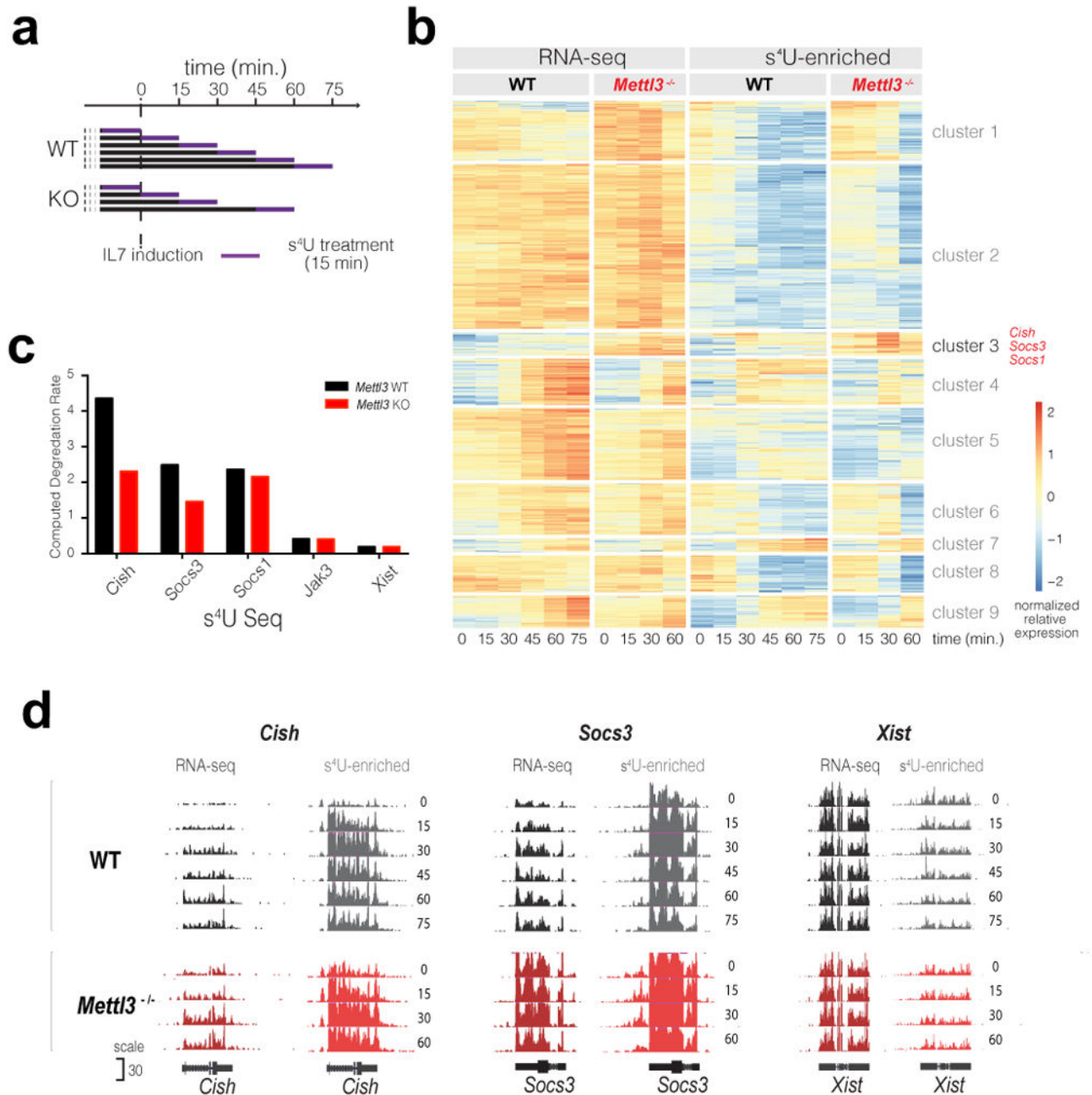


Figure 4. m⁶A specifically target a group of immediate-early genes for degradation upon IL-7 stimulation

a, s4U-Seq experiment overview. **b**, Heatmap showing the results of clustering that normalizes transcript expression levels with significant changes after IL-7 induction and differences between WT and *Mettl3*^{-/-}. Cluster 3 contains 34 transcripts with similar expression profiles including *Cish*, *Socs3* and *Socs1*. **c**, Computed RNA degradation rates from s4U-Seq data. **d**, Read density for total RNA and s4U-enriched RNA at the indicated genes for WT and *Mettl3*^{-/-} samples after IL-7 stimulation.